

AsteroFLAG: first results from hare-and-hounds Exercise #1

W. J. Chaplin^{1,*}, T. Appourchaux², T. Arentoft³, J. Ballot⁴, J. Christensen-Dalsgaard³, O. L. Creevey^{5,6}, Y. Elsworth¹, S. T. Fletcher⁷, R. A. García⁸, G. Houdek⁹, S. J. Jiménez-Reyes⁶, H. Kjeldsen³, R. New⁷, C. Régulo^{10,6}, D. Salabert¹¹, T. Sekii¹², S. G. Sousa^{13,14}, T. Toutain¹, and the rest of the asteroFLAG group¹⁵

¹ School of Physics and Astronomy, University of Birmingham, Edgbaston, Birmingham, B15 2TT, UK

² Institut d'Astrophysique Spatiale (IAS), Batiment 121, F-91405, Orsa Cedex, France

³ Department of Physics and Astronomy, University of Aarhus, DK-8000 Aarhus C, Denmark

⁴ Max-Planck-Institut für Astrophysik, Karl-Schwarzschild-Str. 1, Postfach 1317, 85741, Garching, Germany

⁵ High Altitude Observatory, National Center for Atmospheric Research, Boulder, CO 80301, USA

⁶ Instituto de Astrofísica de Canarias, E-38200, La Laguna, Tenerife, Spain

⁷ Faculty of Arts, Computing, Engineering and Sciences, Sheffield Hallam University, Sheffield S1 1WB, UK

⁸ DAPNIA/CEA, CE Saclay, FR-91191 Gif-sur-Yvette Cedex, France

⁹ Institute of Astronomy, University of Cambridge, Cambridge CB3 0HA, UK

¹⁰ Dpto. de Astrofísica, Universidad de La Laguna, La Laguna, 38206, Tenerife, Spain

¹¹ National Solar Observatory, 950 North Cherry Avenue, Tucson, AZ 85719, USA

¹² National Astronomical Observatory of Japan, Mitaka, Tokyo, 181-8588, Japan

¹³ Centro de Astrofísica Universidade do Porto, 4150-762 Porto, Portugal

¹⁴ Departamento de Matemática Aplicada, Faculdade de Ciências da Universidade do Porto, Portugal

¹⁵ From a further 4 institutes

Received 20 Oct 2007, accepted XX Xxx 200X

Published online later

We report on initial results from the first phase of Exercise #1 of the asteroFLAG hare and hounds. The asteroFLAG group is helping to prepare for the asteroseismology component of NASA's Kepler mission, and the first phase of Exercise #1 is concerned with testing extraction of estimates of the large and small frequency spacings of the low-degree p modes from Kepler-like artificial data. These seismic frequency spacings will provide key input for complementing the exoplanet search data.

© 0000 WILEY-VCH Verlag GmbH & Co. KGaA, Weinheim

1 Introduction

With the recent launch of CoRoT (Baglin et al. 2006), the upcoming launch of Kepler (Basri et al. 2005), and continuation of observations by ground-based teams (Bedding & Kjeldsen 2006, 2007) and MOST (Matthews et al. 2007), we stand on the threshold of a critical expansion of asteroseismology of Sun-like stars, the study of stellar interiors by observation of their global acoustic modes of oscillation. Sun-like oscillations give a very rich spectrum allowing the internal structures and dynamics to be probed down into the stellar cores to very high precision. Asteroseismic observations of many stars will allow multiple-point tests of crucial aspects of stellar evolution and dynamo theory.

The aims of the asteroFLAG collaboration are to help the community to refine existing methods for analysis of the asteroseismic data on Sun-like stars and to develop new ones. The asteroFLAG group is diverse. There is expertise from those involved in the cutting-edge ground-based asteroseismic observations; members of the CoRoT Data Anal-

ysis Team (DAT) (see Appourchaux 2003; 2006a, b); members of the Kepler Asteroseismology Science Consortium (KASC) (Christensen-Dalsgaard et al. 2007); leading theoreticians on the interior structures of stars and Sun-like oscillations; and those involved in the analysis of the so-called “Sun-as-a-star” helioseismology data, for which the analysis methods have direct application to the asteroseismic case (e.g., Chaplin et al. 2006).

The input data for probing stellar interiors are the mode parameters, such as individual frequencies, frequency splittings, linewidths and powers. For those stars where measurement of individual mode parameters is difficult, the input data will be the likes of average frequency spacings. Accurate mode parameter data are a vital prerequisite for robust, accurate inference on the internal structures of the stars. Our objectives are to test aspects of the complete analysis pipelines for stars, i.e., extraction of estimates of the mode parameters from observations, through to procedures used to draw inference on the fundamental stellar properties and the internal structures.

Initially, asteroFLAG is concentrating on main-sequence stars and is conducting the work within a *hare-and-hounds*

* Corresponding author: e-mail: w.j.chaplin@bham.ac.uk

framework. Sets of artificial asteroseismic data will be made by *hares* in the group, to simulate observations by different instruments (both ground and space-based). Information for constructing the artificial data comes from several sources, including full stellar evolutionary codes and analytical descriptions of the stochastic excitation and damping of the Sun-like oscillations. The artificial data are then being analyzed by other members of the group, who are the *hounds*.

AsteroFLAG is already involved in helping to prepare for the asteroseismology component of NASA's Kepler mission. In this paper, we report on the initial results of the first phase of Exercise #1 of the asteroFLAG hare and hounds, which is concerned with extraction of the large and small frequency spacings of the p-mode spectra, from Kepler-like observations of main-sequence stars.

2 Exercise #1 of asteroFLAG hare and hounds: Observations by Kepler

In addition to searching for Earth-like exoplanets (via the transit method), NASA's Kepler mission will also provide an unprecedented opportunity to study a wide range of stars by asteroseismology. The Kepler Asteroseismology Investigation (KAI) will be arranged around the Kepler Asteroseismic Science Operations Centre (KASOC), which will be based at the Danish AsteroSeismology Centre (DASC, Aarhus) (Christensen-Dalsgaard et al. 2007). There is wide participation from the international community in the Kepler Asteroseismology Science Consortium (KASC).

The nominal mission lifetime is ≈ 4 years. There will potentially be a few hundred Sun-like asteroseismic targets, with about 100 eventually getting continuous coverage over the entire mission. This last element is crucial, in that it is only from extended observations that certain scientifically rich, but extremely subtle, elements of the oscillation spectra can be measured, e.g., frequency asymmetries of mode peaks (diagnostics of granulation) and frequency asymmetries of mode splittings (diagnostics of magnetic dynamo signatures).

The first phase of Exercise #1 is concerned with testing extraction of estimates of the large and small frequency spacings of the low-degree modes. These seismic frequency spacings will provide key results for complementing the exoplanet search data (e.g., see Stello et al. 2007a): the large spacings provide tight constraints for estimating radii of the exoplanet host stars, which may then be used to give precise estimates of the exoplanet radii; while the small spacings may be used to help constrain ages of the host stars. The ultimate goal of Exercise #1 will be to estimate the radii of the artificial stars, using the estimated spacings as one of the key data inputs.

When mode peaks observed in the power frequency spectra are of sufficient quality it will be possible to obtain extremely precise estimates of *individual* mode frequencies, for example by application of peak-bagging fitting methods developed for Sun-as-a-star data. Use of individual mode

frequencies will then allow even tighter constraints to be placed on the stellar radii, and we will also test such analyses using the artificial asteroFLAG datasets.

Our intention is to provide input and guidance to the KASC to help develop a robust strategy, or recipe, for estimation of stellar radii under different dataset scenarios (i.e., for different intrinsic stellar properties and noise levels). In this paper we show initial results from Exercise #1 on estimation of the large spacings. WJC and four other colleagues (T. Appourchaux, GH, RN and TS) have thus far acted as the hares, and have generated artificial data on a selection of main-sequence stars for other members of the group, the hounds, to analyse blind. The hounds who have returned results thus far are T. Arentoft, JB, OC, STF, RAG, SJJ-R, CR and DS.

2.1 The asteroFLAG simulator

A detailed description of the asteroFLAG simulator will be presented elsewhere (Chaplin et al., in preparation). Here, we note briefly the main elements of the simulator. These elements are shown visually in block diagram form in Figure 1, with the simulator configured for observations made in intensity. Each timeseries comprises photometric perturbations from: p modes; granulation noise; active region noise; and photon shot and instrumental noise.

2.1.1 Fixing the input parameters

We have used the Aarhus stellar evolution code (ASTEC) and the adiabatic pulsation code ADIPLS to compute theoretical adiabatic pulsation frequencies of the artificial stars (Christensen-Dalsgaard 2007a, b). We use results on stellar equilibrium and pulsation calculations, which have been applied in detail to the Sun and other Sun-like stars (Balmforth 1992; Houdek et al. 1999; Houdek & Gough 2002), to estimate the excitation rates and damping rates of the p modes. The amplitudes of the stochastically excited modes were obtained in the manner of Chaplin et al. (2005, 2007a).

Latitudinally dependent surface rates of rotation were fixed according to empirical laws, with scaling fixed by the colour, $B-V$, and age of the star (Aigrain, Favata & Gilmore 2005; Cardini & Cassatella 2007; Donahue et al. 1996; Reiners & Schmidt 2003). (The $B-V$ colour was derived from the effective temperature, T_{eff} , and metallicity of the model, using the empirical relations of Alonso, Arribas & Martínez-Roger 1996.) Rotation kernels calculated from the stellar models, together with simple internal rotation laws, were then used to determine the rotational frequency splittings. We note that the rotational frequency splittings of the models used in Exercise #1 were fixed deliberately at Sun-like, twice Sun-like and three-times Sun-like values (see Section 2.2 below).

Stellar-cycle effects were not included in the artificial timeseries data described in this paper. However, the asteroFLAG simulator can include these effects. The outline implementation is as follows. A commonly used indicator of

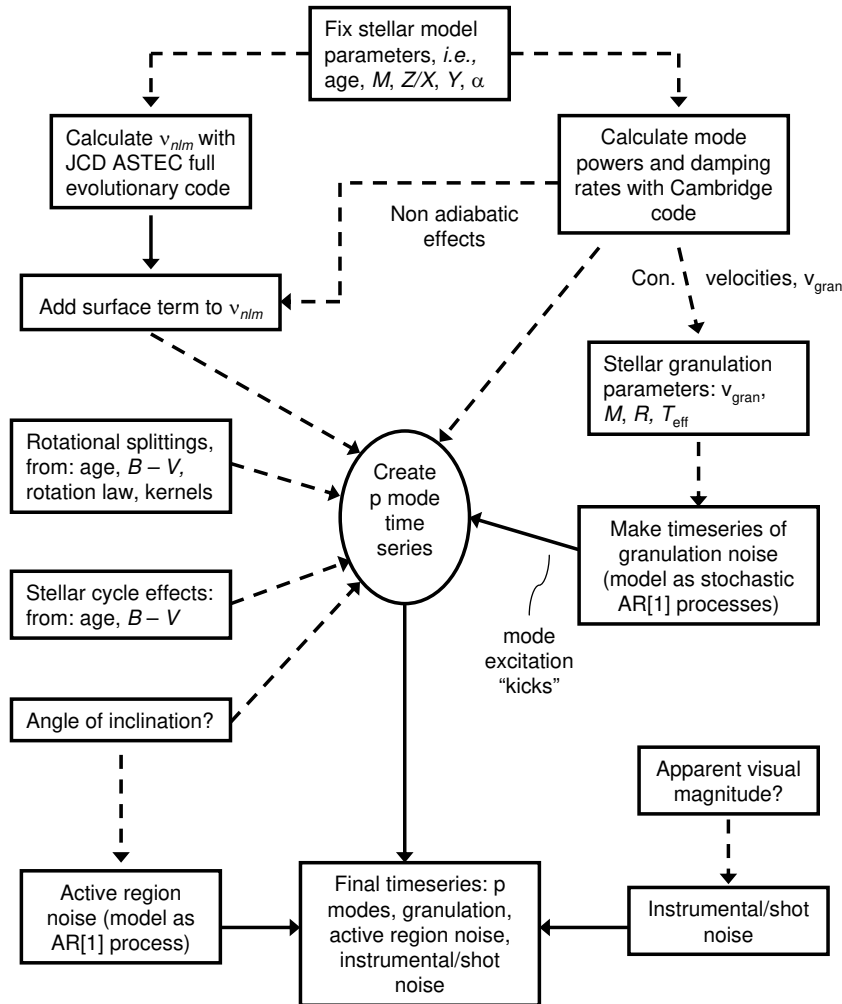


Fig. 1 The main elements of the asteroFLAG simulator.

surface activity on stars is the Ca II H & K index. This index is usually expressed as R'_{HK} : the average fraction of the star's total luminosity that is emitted in the H & K line cores (having been corrected for the photospheric component). We use scaling relations due to Noyes (1983) and Noyes et al. (1984), which require $B - V$ and the surface rate of rotation, to estimate R'_{HK} for our artificial stars. Scaling laws, based on fits to observations (Radick et al. 1995; Saar & Brandenburg 2002) of stellar-cycle variability in R'_{HK} were then used to fix the amplitudes, $\Delta R'_{\text{HK}}$, and the periods of

the stellar cycles. Cycle amplitudes $\Delta R'_{\text{HK}}$ were then converted to equivalent p-mode parameter shifts (e.g., in frequency, power and damping) in the manner described in Chaplin et al. (2007a). There is also the provision to include effects of acoustic asphericity, from the non-homogeneous distribution of the simulated near-surface activity (again, see Chaplin et al. 2007a).

Mode visibilities were calculated according to Christensen-Dalsgaard & Gough (1982). We also allowed for limb darkening, and used the limb-darkening laws of van Hamme

(1993) to describe variation of the limb-darkening properties from one star to another. These laws use the effective temperature, T_{eff} , and the surface gravity to fix the coefficients describing the limb-darkening.

To estimate the standard deviation and timescale of the granulation, we have used scaling laws, and scaled against solar values (see also Stello et al. 2007b; Kjeldsen & Bedding, in preparation). The solar values were estimated from analysis of a multi-year timeseries of solar intensity observations made by the VIRGO/PMO6 instrument on board the *ESA/NASA SOHO* spacecraft. We have assumed that the standard deviation of the brightness fluctuations scales in inverse proportion to the square root of the number of convective cells on the surface of the star (we assume the cells are statistically independent; see also Ludwig 2006). The characteristic size of cells was assumed to scale with the product of the mixing length parameter and the isothermal scale height at the surface of the star. The brightness fluctuations associated with individual cells were assumed to scale with the surface velocities associated with the convection, which came from the stochastic excitation models that were used to predict the mode excitation and damping rates. To estimate the timescale of the granulation we assumed it scales in inverse proportion to the acoustic cut-off frequency of the star.

The standard deviation of the active region noise was assumed to scale with R'_{HK} , in the manner described by Aigrain, Favata & Gilmore (2005). We also allowed for the effect of the angle of inclination of the star, having assumed the active-region signal was confined within certain bands of stellar latitude, using the work of Knaack et al. (2001) as a guide. We assumed the timescale of the active-region signal scaled with the period of rotation of the star.

For the photon shot noise, we used the latest estimates of the expected precision of the Kepler observations at different m_v . These data were provided to HK by the Kepler team.

2.1.2 Generation of the artificial data

Components due to granulation and active regions were generated in the time domain using a stochastic, autoregressive model of the AR[1] type (e.g., see Koen 2005).

We used code based on the latest version of the solarFLAG (Chaplin et al. 2006) timeseries generation code to make the p-mode timeseries (the solarFLAG generator is described in Chaplin et al., in preparation). Each (n, l, m) component was generated in the time domain. Components were modeled as forced, damped harmonic oscillators, re-excited at frequent intervals (here, every minute). The oscillators were re-excited by a timeseries of ‘kicks’ made from the granulation noise. Kicks given to overtones of the same (l, m) were correlated. Implicit in this approach is the assumption that on the Sun, the excitation function of a mode of a given (l, m) is the same as the component of the granulation that has the same spherical harmonic projection over the corresponding range in frequency (Toutain, Elsworth & Chaplin

2005). Correlations of the excitation of different overtones, coupled with the later addition of granulation noise to the p-mode timeseries, gave rise to asymmetries of the resonant peaks in the power frequency spectrum (asymmetries that are displayed by the solar p modes).

To give an idea of the expected quality of the Kepler observations, Figure 2 shows how Kepler would see the Sun, according to the asteroFLAG simulator, were the Sun to be observed continuously for 4 yr at apparent visual magnitude $m_v = 9$. This is at the bright m_v end of the target range, which extends down to brightness $m_v \sim 15$ (e.g., Christensen-Dalsgaard et al. 2007).

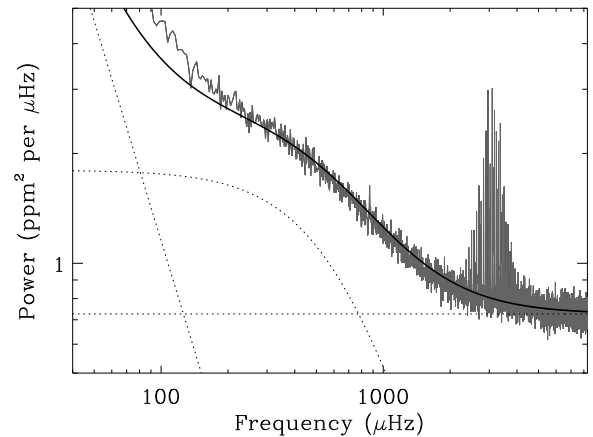


Fig. 2 How Kepler would see the Sun, according to the asteroFLAG simulator, were it to be observed continuously for 4 yr at apparent visual magnitude $m_v = 9$. The power frequency spectrum of the timeseries is rendered in light grey, with the most prominent modes observed at frequencies around $\sim 3000 \mu\text{Hz}$. The individual limit contributions of photon shot noise, granulation, and active-region noise are shown as the dotted lines. The total contribution of these three ‘noise’ components is plotted as a dark, continuous line.

2.2 Data for Exercise #1

For the first phase of Exercise #1, we have prepared timeseries of Kepler-like data on 3 artificial stars. We have named the artificial stars Pancho, Boris and Katrina¹ Here, we present results on a total of twenty-eight 4-yr timeseries prepared for each star. These timeseries covered all possible combinations of the following:

- Four different apparent visual magnitudes, $m_v = 9, 11, 13$ and 15 ;

¹ The chosen names are names of cats with whom several of the authors are acquainted. Given the origins of the naming of our stars, it has been suggested that our hare-and-hounds exercises should instead be called cat-and-mouse exercises.

- Three different angles of stellar inclination, $i = 0, 30$ and 60 degrees;
- Three different mean internal rates of rotation: Sun-like, twice Sun-like, and three-times Sun-like;

We note that the same realization noise was always used to excite the overtones of each (l, m) of a given star, regardless of the dataset; however, different realizations of the photon shot noise were added at each of the different apparent magnitudes. As indicated previously, the timeseries did not include stellar-cycle-like effects.

These multiple timeseries were intended to help the hounds test their analysis codes, and so the hares also passed to the hounds a priori information on the inclinations and rotation rates of the datasets. It is in the next phase of Exercise #1 that data will be released at only one m_v per star, on a selection of new stars, thereby providing true blind tests for the hounds. We comment below on the potential impact on the results of the additional a priori information given by having multiple timeseries on each star.

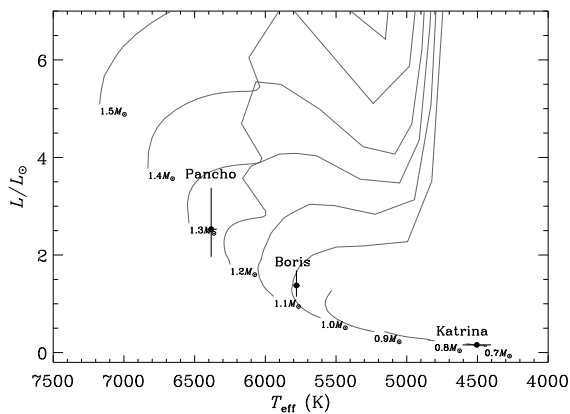


Fig. 3 Locations of the stars Pancho, Boris and Katrina (see figure annotation) on a temperature-luminosity diagram, with locations inferred from the traditional data released on the stars. Here, we used the artificial parallax data for $m_v = 9$. The grey lines show evolutionary tracks, made with the Padova models (Bonatto, Bica & Girardi 2004; Girardi et al. 2002, 2004).

In addition to the timeseries data, the hares also released ‘traditional’ data on the stars, appropriate to each apparent visual magnitude, m_v . The traditional data were: parallaxes, π , metallicities, $[\text{Fe}/\text{H}]$, and effective temperatures, T_{eff} . (Full details on these data will be given in a separate paper.) Figure 3 shows the location of the artificial stars on a temperature-luminosity diagram. The positions have been inferred using the traditional data (with the parallax for $m_v = 9$). Here, we followed procedures the hounds would need to adopt to convert from absolute visual to absolute bolometric magnitude (we used the bolometric corrections of Flower 1996). The locations of the stars in Figure 3 in-

dicates that Pancho is intrinsically the brightest star; whilst Katrina is intrinsically the faintest star.

Figure 4 shows how Kepler would see Pancho (left-hand panel), Boris (middle panel) and Katrina (right-hand panel), according to the asteroFLAG simulator, were the artificial stars to be observed continuously for 4 yr at apparent visual magnitude $m_v = 11$. Pancho shows the strongest p-mode amplitudes of the three stars, while Katrina has the weakest modes.

3 Results

The hounds made up six teams: JB, RAG and SJJ-R formed one team; while T. Arentoft, OC, STF, CR and DS worked individually. The hounds extracted estimates of the large frequency spacings using various methods. T. Arentoft used a Matched Filter approach, which is similar to methods applied in searches for exoplanet transits (see Christensen-Dalsgaard et al. 2007). The other hounds used either Fourier transforms of the power frequency spectra (one hound actually worked on autocorrelation functions of the timeseries) or autocorrelations of the power frequency spectra (e.g., see Scargle 1989; Ransom, Eikenberry & Middleditch 2002). We also note that JB, RAG and SJJ-R worked on ‘denoised’ power frequency spectra of timeseries, using the curvelet transform (Lambert et al. 2006). For analysis of several timeseries, some hounds divided the timeseries into shorter pieces. Power frequency spectra of these shorter pieces were then computed and co-added for subsequent analysis.

In all cases the hounds had to make choices over what ranges in frequency to use for the analyses. Estimates of the large spacings are affected to some extent by the range that is chosen, because the large spacings are frequency dependent. The angle of inclination and the magnitudes of the mode frequency splittings – both of which affect the appearance of the mode peaks, both within multiplets, and from one degree l to another – will also have a subtle effect on the results. The estimates may also be affected by the implementation of the analysis, for example from the manner in which peaks in the autocorrelation, or Fourier transform, of the power frequency spectrum are fitted to yield the estimated spacings. Before we show the main results of the hounds, we first illustrate the impact of some of the effects listed here.

We computed the smooth, noise-free ‘limit’ power frequency spectrum of each timeseries, and then analysed each noise-free power frequency spectrum to estimate the large spacings. When we analysed each spectrum, we used the range in frequency that each hound chose when they analysed that same spectrum. We estimated the spacings using both of the basic methods adopted by the hounds. The results that are given correspond to a ‘best case scenario’, in that there is no noise in the power frequency spectrum. We note that our implementation of the methods most likely differed in detail from implementations of the hounds. The results provide a guide to differences we might expect from

the free choice of the frequency range and analysis method, and of the inclination and mode frequency splittings. It is worth adding that the frequency range selected for analysis is information one would aim to use in determining the stellar radius, even if it was not possible to measure individual mode frequencies reliably.

Figure 5 shows the estimated spacings extracted from noise-free power frequency spectra of the artificial star Boris. Each symbol is used to show results for the frequency ranges chosen by a particular hound. The left-hand panel shows results from using the autocorrelation of the power frequency spectrum; while the right-hand panel shows results from using the Fourier transform of the power frequency spectrum. Agreement between the results is of course very good, so much so that it is hard to tell results apart for the autocorrelation method. However, there are differences present, which are in some cases as large as $\approx 0.75\%$ of the mean spacings. We consider below how scatter in the large spacing estimates translates to uncertainty in estimates of stellar radii.

The main results on the large frequency spacings $\Delta\nu$ are shown for each star in Figures 6, 7 and 8. The various symbols show results for different hounds. (JB, RAG and SJJ-R concentrated on developing application of the curvelet technique, and have returned results initially for Pancho only.) A first look at the results showed that there was no clear, systematic dependence of the estimated spacings on either the inclination or the internal rate of rotation. We therefore decided not to differentiate between these parameters when plotting the results (so that all estimates of $\Delta\nu$ for a given star are plotted on the same graph).

It is important to recognise that choices made for the higher noise (larger m_v) spectra may have been influenced by results on the lower noise (smaller m_v) spectra. Perhaps the most important choice is the part of the power frequency spectrum that is selected for subsequent analysis. The choice can be less than straightforward when the mode peaks are not readily apparent in the power frequency spectrum. Under such circumstances it may still be possible to extract a robust estimate of the spacing provided the right part of the spectrum is selected. This is the most obvious example of where our hounds will have learned from, and therefore benefited by, their selections made for the lower noise spectra.

We should add that information included with the results returns (together with the results themselves) suggests that the hounds did attempt to treat each timeseries on its own merits. But this may not always have been possible where the choice of frequency range was concerned. For analysis on real stars, and in the absence of prominent mode peaks in the power frequency spectrum, one would seek to use already-known traditional information on the star to help fix suitable ranges in frequency to analyse. Furthermore, the curvelets used by JB, RAG and SJJ-R, certainly help in cleaning up the raw spectra to reveal the presence of any modes.

Let us now turn to the main results. The top left-hand panel of each figure shows estimates of the large spacings returned by the hounds. The error bars show the uncertainties in $\Delta\nu$ required to give 1% uncertainties on the inferred radii of the stars. These values follow straightforwardly from the dependence of the mean spacing on the mean density of the star (e.g., Kjeldsen & Bedding 1995):

$$\Delta\nu \propto M^{1/2} R^{-3/2}, \quad (1)$$

so that

$$\delta R/R = -2/3 \delta\Delta\nu/\Delta\nu. \quad (2)$$

The absolute uncertainty in $\Delta\nu$ required to give a 1% uncertainty in R is therefore given by:

$$\delta\Delta\nu_{1\%} = 0.01 \times 3/2 \Delta\nu = 0.015 \Delta\nu. \quad (3)$$

The top right-hand panels of each figure again show estimates of the large spacings, but plotted over a much larger range on the ordinate to show poor estimates of the spacings.

The bottom left-hand panels of each figure show estimated spacings extracted (by WJC) from analysis of autocorrelations of noise-free power frequency spectra (see Figure 5 and discussion above). The different symbols show results for the frequency ranges chosen by particular hounds. These results serve as a useful “noise-free” reference for the main (noisy timeseries) results shown in the top panels of each figure.

Finally, the bottom right-hand panels show estimates of the uncertainties on the large spacings returned by the hounds. The dashed lines show standard deviations of the results of the hounds at each apparent visual magnitude, m_v . The dotted lines again show the uncertainties in $\Delta\nu$ required to give 1% uncertainties on the inferred stellar radii. The most striking aspect of the uncertainty estimates is that they cover such a wide range.

4 Discussion

How should we interpret the precision in the results (i.e., the observed scatter between hounds), and the uncertainty data plotted in the bottom right-hand panel of each figure? In reaching a conclusion we need to remember that all datasets on a given star had the same mode realization noise, but different shot noise.

At the brighter magnitudes (lower noise spectra), scatter between hounds is dominated by differences in implementation of the analysis (what we might term *reduction* noise), which includes the impact of the different frequency ranges chosen by the hounds (see lower left-hand panels of Figures 6 to 8). The magnitude of this observed scatter is larger than the characteristic internal precision on the estimated spacings. By *internal* precision, we mean the typical precision we would expect to get were one of the hounds to analyse many datasets having different shot *and* mode realization noise. For example, T. Arentoft analyzed several fully independent timeseries realizations of Boris (made by

WJC), and found that the characteristic internal precision on the estimated spacings was $\sim 0.04 \mu\text{Hz}$ at $m_v = 9$, and $\sim 0.20 \mu\text{Hz}$ at $m_v = 11$. The observed scatter between hounds is $\approx 0.5 \mu\text{Hz}$ at both magnitudes. At the fainter magnitudes, where scatter between hounds increases, the influence of different realizations of the shot noise comes into play, and the internal precision also drops.

The quoted uncertainties should give robust estimates of the internal precision. However, it is clear from Figures 6 to 8 that the quoted values cover a wide range at each m_v . Some of the hounds' uncertainties were very much smaller even than the expected internal precision. In several cases, this may have been because those estimates came from standard least-squares fits to autocorrelations of the power frequency spectra, where no account had been taken of the strong correlations present in the autocorrelation functions. (See also Chaplin et al. 2007b, for discussion of a similar problem, using the cross correlation function.)

5 Conclusion

The following conclusions may be drawn from the results:

1. It is possible to extract robust estimates of the large frequency spacings, $\Delta\nu$, for many of the timeseries we made. Estimated spacings of the different hounds, returned at values of apparent visual magnitude where robust estimation is possible, show agreement at a level typically better than 1%.
2. The observed level of agreement implies a contribution to the uncertainty on inferred stellar radii of typically a few tenths of 1%.
3. Scatter in the results increases significantly at $m_v = 15$ for Pancho; at $m_v \geq 13$ for Boris; and at $m_v > 9$ for Katrina. Indeed, for the intrinsically fainter Katrina no results on the spacings were returned at $m_v \geq 11$.
4. The observed scatter between hounds for the brighter stars tends to be larger than the characteristic internal precision expected, given the intrinsic quality of the data. The main contribution to this additional scatter appears to be reduction noise (i.e., differences in implementation of the analysis).
5. Estimation of uncertainties in the large spacings, from fits made to prominent peaks in the autocorrelation of the power frequency spectrum, must make proper allowance for the strong correlations that are present in the autocorrelation function.

The next phase of the exercise will involve true blind tests on single timeseries of new stars. We then intend to use the results, together with further tests on the data here, to inform development and refinement by the KASC of the analysis pipeline for extracting the frequency spacings. The results of the asteroFLAG exercises also need to be understood in the context of the Kepler simulations undertaken at Aarhus (see Christensen-Dalsgaard et al. 2007).

Acknowledgements. We are extremely grateful to the International Space Science Institute (ISSI) for support provided by a workshop programme award. This work was also supported by the European Helio- and Asteroseismology Network (HELAS), a major international collaboration funded by the European Commission's Sixth Framework Programme. We thank the VIRGO/SOHO team, whose data we used. SOHO is a mission of international cooperation between ESA and NASA.

References

- Aigrain S., Favata F., Gilmore G., 2004, *A&A*, 414, 1139
 Alonso A., Arribas S., Martínez-Roger C., 1996, *A&A*, 313, 873
 Appourchaux T., 2003, *Ap&SS*, 284, 109
 Appourchaux T., Berthomieu G., Michel E. et al, 2006a, in *The CoRoT Mission*, A. Baglin, J. Lochard, M. Fridlund, L. Conroy eds., Publication ESA SP-1306, p. 429
 Appourchaux T., Berthomieu G., Michel E. et al, 2006b, in *The CoRoT Mission*, A. Baglin, J. Lochard, M. Fridlund, L. Conroy eds. Publication ESA SP-1306, p. 377
 Baglin A., Michel E., Auvergne M., and the CoRoT Team, 2006, in: *Beyond the Spherical Sun, SOHO18/GONG 2006/HELAS I*, eds. K. Fletcher, M. J. Thompson, ESA SP-624, Sheffield, UK, p. 34
 Balmforth N.J., 1992a, *MNRAS*, 255, 603
 Balmforth N.J., 1992b, *MNRAS*, 255, 639
 Basri G., Borucki W. J., Koch D., 2005, *New Astronomy Reviews*, 49, 478, 2005
 Bedding T. R., Kjeldsen H., 2006, in: *Beyond the Spherical Sun, SOHO18/GONG 2006/HELAS I*, eds. K. Fletcher, M. J. Thompson, ESA SP-624, Sheffield, UK, p. 25
 Bedding T. R., Kjeldsen H., 2007, *CoAst*, 350, 106
 Bonatto Ch., Bica E., Girardi L., 2004, *A&A*, 415, 571
 Cardini D., Cassatella A., 2007, *ApJ*, 666, 393
 Chaplin W. J., Houdek G., Elsworth Y., Gough D. O., Isaak G. R., New R., 2005, *MNRAS*, 360, 859
 Chaplin W. J., et al., 2006, *MNRAS*, 369, 985
 Chaplin W. J., Elsworth Y., Houdek G., New R., 2007a, *MNRAS*, 377, 17
 Chaplin W. J., Elsworth Y., Miller B. A., New R., Verner G. A., 2007b, *ApJ*, 659, 1749
 Christensen-Dalsgaard J., Gough D. O., 1982, *MNRAS*, 198, 141
 Christensen-Dalsgaard J., 2007a, *Astrophys Space Sci*, in the press, arXiv:07103114v1
 Christensen-Dalsgaard J., 2007b, *Astrophys Space Sci*, in the press, arXiv:07103106v1
 Christensen-Dalsgaard J., Arentoft T., Brown T. M., Gilliland R. L., Kjeldsen H., Borucki W. J., Koch D., 2007, *CoAst*, 150, 350
 Donahue R. A., Saar S. H., Baliunas S. L., 1996, *ApJ*, 466, 384
 Flower P. J., 1996, *ApJ*, 469, 355
 Giradi L., Bertelii G., Bressnan A., Chiosi C., Grönweggen M. A. T., Marigo P., Salasnich B., Weiss A., 2002, *A&A*, 391, 195
 Giradi L., Grebel E. K., Odenkirchen M., Chiosi C., 2004, *A&A*, 422, 205
 Houdek G., Balmforth N. J., Christensen-Dalsgaard J., Gough D. O., 1999, *A&A*, 351, 582
 Houdek G., Gough D. O., 2002, *MNRAS*, 336, L65
 Kjeldsen H., Bedding T. R., 1995, *A&A*, 293, 87
 Knaack R., Fligge M., Solanki S. K., Unruh Y. C., 2001, *A&A*, 376, 1080

- Koen C., 2005, *MNRAS*, 361, 887
- Lambert P., Pires S., Ballot J., García R. A., Starck J.-L., Turck-Chièze S., 2006, *A&A*, 454, 1021
- Ludwig H.-G., 2006, *A&A*, 445, 661
- Matthews J., et al., 2007, *CoAst*, 350, 333
- Noyes R. W., 1983, in: *Solar and Stellar Magnetic Fields: Origins and Coronal Effects*, IAU Symp., 102, 133
- Noyes R. W., Hartmann L. W., Baliunas S. L., Duncan D. K., Vaughan A. H., 1984, *ApJ*, 279, 763
- Radick R. R., Lockwood G. W., Skiff B. A., Thompson D. T., 1995, *ApJ*, 452, 332
- Ransom, S. M., Eikenberry, S. S., Middleditch, J., 2002, *AJ*, 124, 1788
- Reiners A., Schmitt J. H. M. M., 2003, *A&A*, 398, 647
- Saar S. H., Brandenburg A., 2002 *AN*, 323, 357
- Scargle, J. D., 1989, *ApJ*, 343, 874
- Stello D., Kjeldsen H., Bedding T. R., 2007a, in: *Transiting Extrasolar Planets Workshop*, ASP Conf. Series Vol. 366, eds. C. Afonso, D. Weldrake, Th. Henning, San Francisco, p. 247
- Stello D., et al., 2007b, *MNRAS*, 377, 584
- Toutain T., Elsworth Y., Chaplin W. J., 2006, *MNRAS*, 371, 1731
- van Hamme W., 1993, *AJ*, 106, 2096

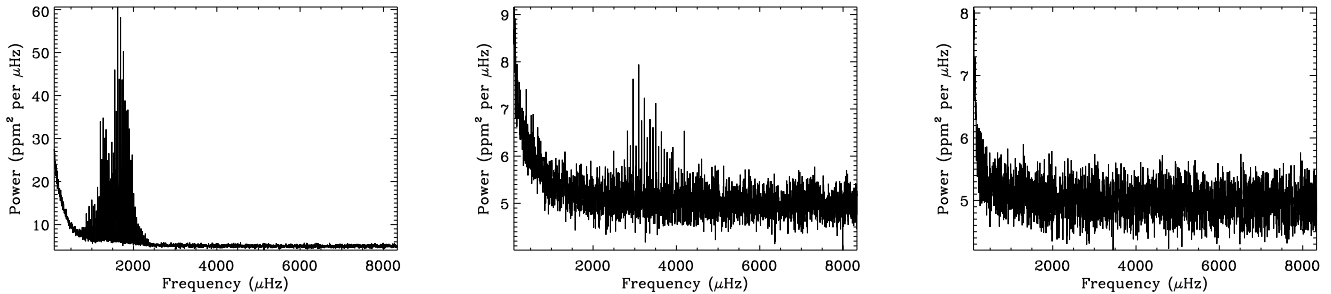


Fig. 4 How Kepler would see Pancho (left-hand panel), Boris (middle panel) and Katrina (right-hand panel), according to the asteroFLAG simulator, were the artificial stars to be observed continuously for 4 yr at apparent visual magnitude $m_v = 11$. The plots show average power frequency spectra, made by dividing the full timeseries into short 4-day segments and co-adding the individual spectra.

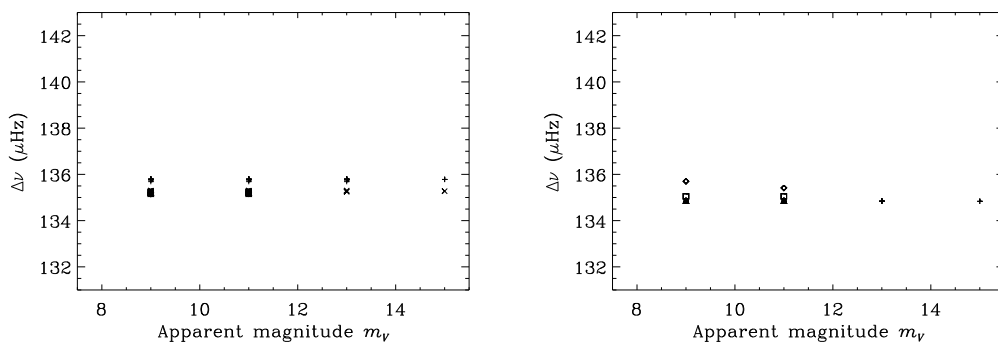


Fig. 5 Estimated spacings extracted from noise-free power frequency spectra of the artificial star Boris. Each symbol is used to show results for the frequency ranges chosen by a particular hound. The left-hand panel shows results from using the autocorrelation of the power frequency spectrum; while the right-hand panel shows results from using the Fourier transform of the power frequency spectrum.

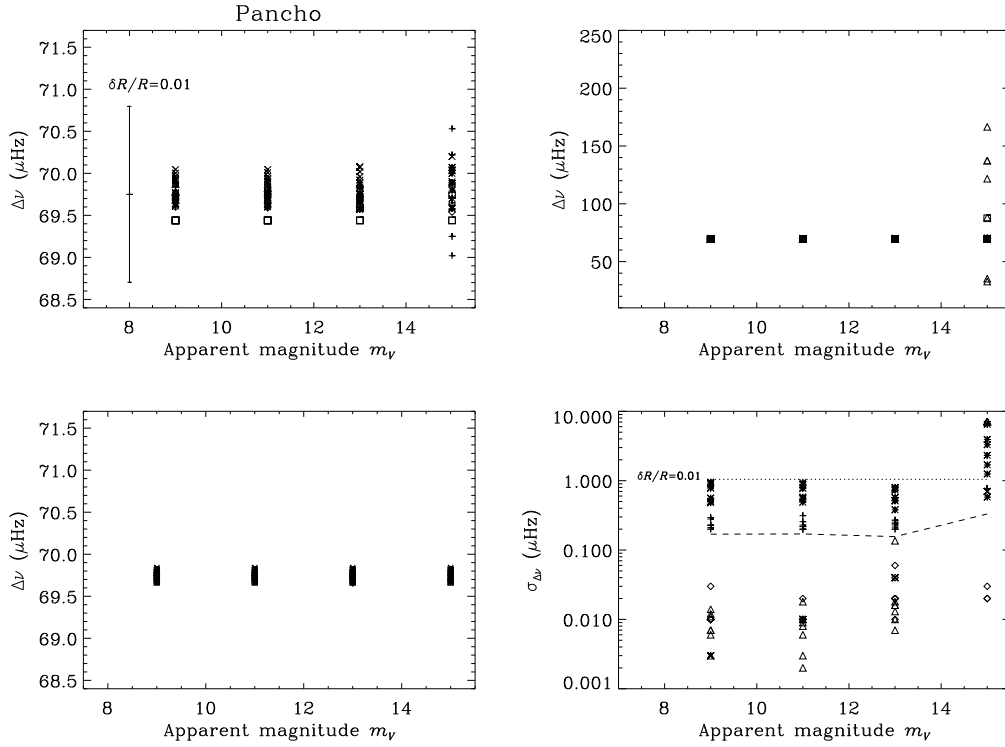


Fig. 6 Results, on estimation of the large spacings, $\Delta\nu$, for artificial timeseries of Pancho. Symbols show results for different hounds. Top left-hand panel: estimates of the large spacings returned by the hounds. The error bar shows the uncertainty in $\Delta\nu$ required to give a 1% uncertainty on the inferred radius of the star. Top right-hand panel: estimates of the large spacings, but plotted over a much larger range on the ordinate to show poor estimates of the spacings. Bottom left-hand panel: estimated spacings extracted from noise-free power frequency spectra by WJC (see Figure 5), using the autocorrelation of the power frequency spectrum. This is the only panel in which symbols do not indicate results for different hounds, but rather the results of WJC for the *frequency ranges* chosen by different hounds. Bottom right-hand panel: estimates of the uncertainties on the large spacings returned by the hounds. The dashed line shows the standard deviation of the results of the hounds at each apparent visual magnitude, m_v . The dotted line again shows the uncertainty in $\Delta\nu$ required to give a 1% uncertainty on the inferred radius of the star.

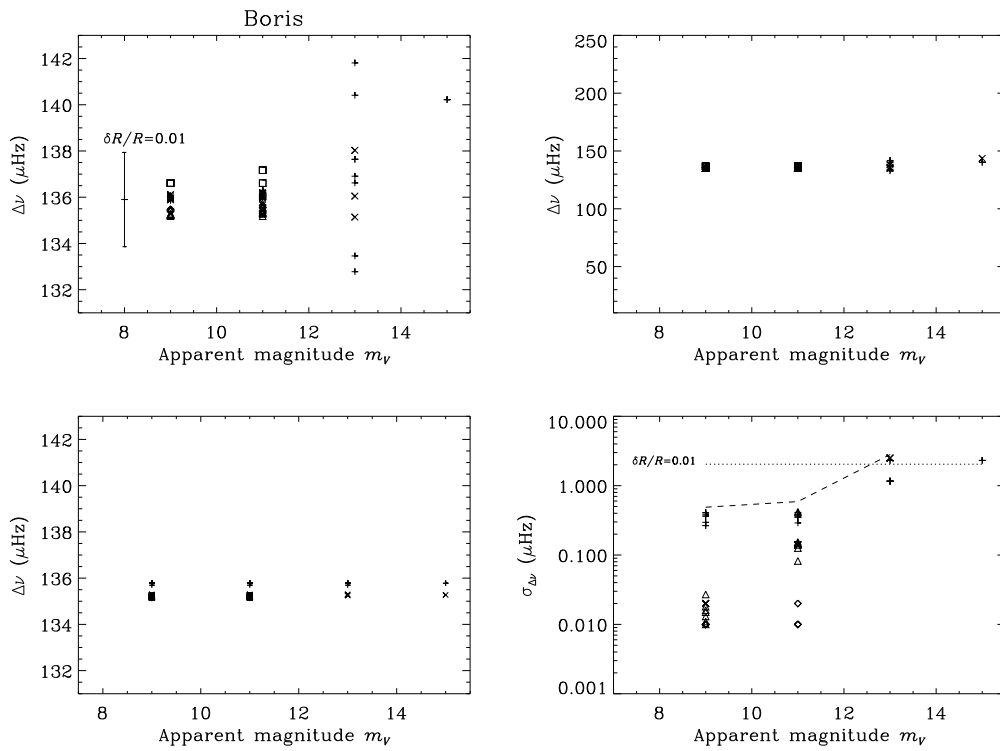


Fig. 7 Results, on estimation of the large spacings, for artificial timeseries of Boris. (Details as per Figure 6.)

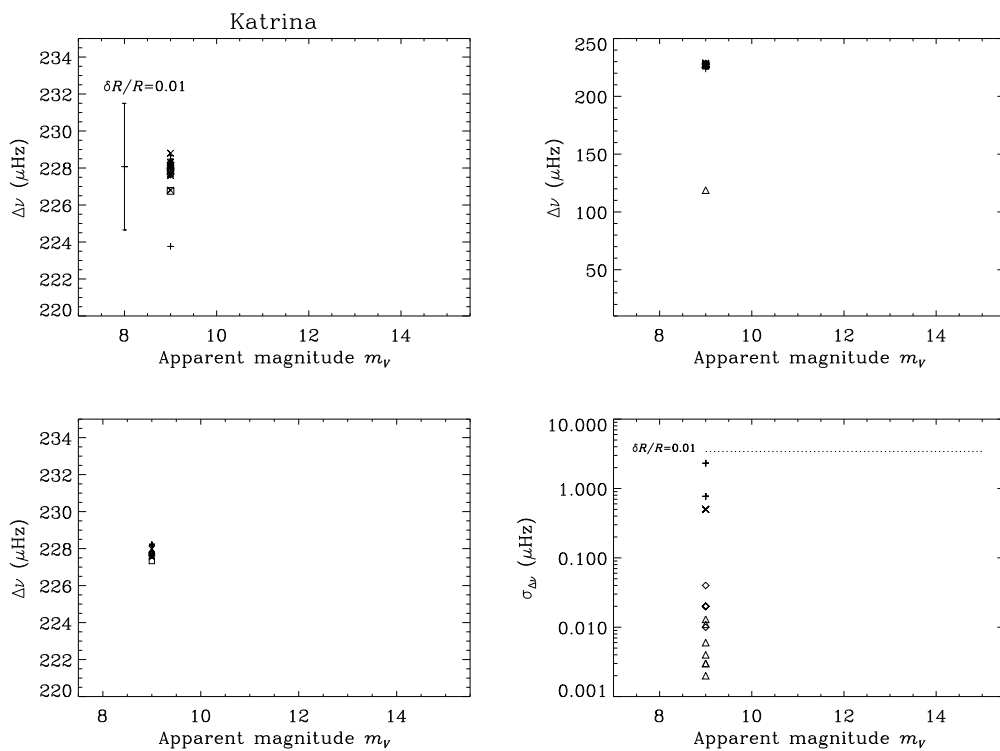


Fig. 8 Results, on estimation of the large spacings, for artificial timeseries of Katrina. (Details as per Figure 6.)